Redox Biology 58 (2022) 102555

Contents lists available at ScienceDirect

Redox Biology

journal homepage: www.elsevier.com/locate/redox

# Ferritin light chain deficiency-induced ferroptosis is involved in preeclampsia pathophysiology by disturbing uterine spiral artery remodelling

Xiaofeng Yang [a,1], Yuzhen Ding [a,1], Lu Sun [a], Meiting Shi [a], Ping Zhang [a], Zhengrui Huang [a], Jingyun Wang [a], Andong He [a], Jian Wang [a], Jiachun Wei [a], Mengyuan Liu [a], Jia Liu [a], Guang Wang [b,***], Xuesong Yang [b,c,**], Ruiman Li [a,*]

[a] Department of Obstetrics and Gynecology, The First Affiliate Hospital of Jinan University, Guangzhou, 510630, China
[b] International Joint Laboratory for Embryonic Development & Prenatal Medicine, Division of Histology and Embryology, Medical College, Jinan University, Guangzhou, 510632, China
[c] Key Laboratory for Regenerative Medicine of the Ministry of Education, Jinan University, Guangzhou, 510632, China

ARTICLE INFO

*Keywords:*
FTL
PE
Uterine spiral artery remodelling
Ferroptosis

ABSTRACT

The proteomic analysis from samples of patients with preeclampsia (PE) displayed a low level of ferritin light chains (FTL), but we do not know what the significance of reduced FTL in PE pathophysiology is. To address this question, we first demonstrated that FTL was expressed in first- and third-trimester cytotrophoblasts, including extravillous trophoblasts (EVTs), of the human placenta. Furthermore, a pregnant rat model of FTL knockdown was successfully established by intravenously injecting adenoviruses expressing shRNA targeting FTL. In pregnant rats with downregulated FTL, we observed PE-like phenotypes and impaired spiral arterial remodelling, implying a causal relationship between FTL downregulation and PE. Blocking ferroptosis with ferrostatin-1 (Fer-1) significantly rescued the above PE-like phenotypes in pregnant rats with FTL knockdown. Furthermore, using trophoblast cell line and chorionic villous explant culture assays, we showed that FTL downregulation induced cell death, especially ferroptosis, resulting in defective uterine spiral artery remodelling. Eventually, this conclusion from the animal model was verified in PE patients' placental tissues. Taken together, this study revealed for the first time that FTL reduction during pregnancy triggered ferroptosis and then caused defective uterine spiral artery remodelling, thereby leading to PE.

## 1. Introduction

Preeclampsia (PE) has been an overriding factor of maternal morbidity and mortality worldwide [1,2]. PE is characterized by new-onset hypertension, fluid retention (oedema), and protein in the urine (proteinuria) after the 20th week of pregnancy [3]. Based on the occurrence time, PE can be classified into two kinds: early-onset PE (before 34 weeks of gestation) and late-onset PE (after 34 weeks of gestation), which are deemed to have different disease entities [4]. Untreated or improperly treated PE could develop into a more serious condition, i.e., eclampsia. Epidemiological studies have shown that the occurrence and development of PE are related to the delay of female reproductive age, the increase in the female obesity rate, and the popularization of assisted reproductive technology. PE-induced vascular injury, including cardiovascular disease (CVD) and/or chronic kidney disease (CKD), results mainly from triggering metabolic syndrome with extensive endothelial dysfunction [5]. Recurrent PE increases the risk of deterioration, i.e., eclampsia. The manifestation of severe PE is often demonstrated by the presence of systemic endothelial dysfunction, as well as damage to liver and kidney functions. In this case, the serum

* The corresponding author.
** The corresponding author. International Joint Laboratory for Embryonic Development & Prenatal Medicine, Division of Histology and Embryology, Medical College, Jinan University, Guangzhou, 510632, China.
*** The corresponding author.
*E-mail addresses:* wangguang7453@126.com (G. Wang), yang_xuesong@126.com (X. Yang), hqyylrm@126.com (R. Li).
[1] Contribute to the work equally.

https://doi.org/10.1016/j.redox.2022.102555
Received 8 September 2022; Received in revised form 9 November 2022; Accepted 23 November 2022
Available online 24 November 2022

levels of sFlt-1 increased, while placental growth factor (PLGF) and vascular endothelial growth factor (VEGF) decreased [6]. Growing evidence shows that PE develops from an excessive maternal intravascular inflammatory response to a pregnancy-related stimulus, which is strong enough to cause a maternal disproportionate response [7]. In other words, PE is associated with an imbalance between proinflammatory and anti-inflammatory in the context of chronic immune activation/inflammation in pregnancy [8].

Please note that the pathological mechanism of PE is not fully understood, although many hypotheses have been proposed thus far [9]. At present, it is hypothesized that inadequate remodelling of maternal uterine spiral arteries and insufficient trophoblast invasion are the key factors leading to PE [10]. With regard to uterine spiral artery remodelling under normal physiological conditions, trophoblasts, which are initially derived from the outermost layers of blastocysts, migrate towards the maternal uterine spiral artery to replace vascular endothelial and smooth muscle cells (VSMCs) (i.e., remodelling process). Briefly, during early human pregnancy, EVTs invade the uterine wall and complete spiral artery remodelling, thereby transforming the spiral artery into large vessels with low resistance. It follows then that the failure of either fetal-derived trophoblast cell invasion or vascular epithelial and/or smooth muscle cell vanishment would greatly contribute to the inadequate remodelling of the uterine spiral artery, which would in turn lead to PE development. During the rapid growth of the placenta, there is a low-oxygen environment because the oxygen gradient plays a very important role in inducing certain types of trophoblast migration, proliferation, and differentiation. Such intermittent hypoxic environments will be improved after the completion of uterine spiral artery remodelling, since completely remodelled uterine arteries dramatically increase blood flow to ensure the needs of the developing foetus. In contrast, inadequate remodelling of the uterine spiral artery restricts the blood supply to the placenta and results in placental hypoxia, thereby increasing the possibility of PE [11], which could be followed by other PE complications, such as late miscarriage and fetal growth restriction [12,13]. Notably, proper uterine spiral artery remodelling is accomplished by disrupting the invasion of EVTs, i.e., VSMCs are appropriately replaced by infiltrating EVTs.

As recently recognized iron-dependent cell death, ferroptosis is dissimilar to other kinds of cell death, such as necrosis and apoptosis. The process of ferroptosis encompasses three primary metabolisms, including thiol, lipid, and iron, which cause iron-dependent production of lipid peroxidation, thereby triggering cell death [14]. In other words, ferroptotic cell death is considered as the accretion of lethal lipid species, which results from the peroxidation of lipids [14]. Hence, ferroptosis can be restricted by the following two major antioxidant systems. One of them is glutathione peroxidase 4 (GPX4), which degrades lipid peroxides through a glutathione-dependent reaction, and the other is ferroptosis suppressor protein (FSP1), which promotes the regeneration of ubiquinone (Coenzyme Q10, CoQ10), which can trap lipid peroxyl radicals [15,16]. As a radical-trapping antioxidant, ferrostatin-1 (Fer-1) (i.e., an inhibitor of ferroptosis) can suppress the generation of ferroptosis (RTA) [17,18].

Ferritin light chain (FTL) is one of two subunits of ferritin, which is composed of a polymer of FTL and ferritin heavy chains (FTH) and plays an important role in maintaining iron haemostasis [19]. FTL consists of 174 amino acids, and its molecular weight is 19 kDa. FTL is deemed to provide acidic residues for iron nucleation on the ferritin molecule [20]. The mutation in FTL will interrupt the dodecahedron structure of ferritin, thereby disrupting its ability to transport iron [20]. The inherited neurodegenerative disease (i.e., neuroferritinopathy) caused by FTL mutations indicated that dysfunction of FTL was associated with neurodegenerative diseases because of redox-active iron deposits in neurological tissue [21,22]. In this study, we investigated the role of FTL in the process of PE development by utilizing a combination of human tissue samples and an FTL-downregulated rat model.

## 2. Materials and methods

### 2.1. Human tissue collection

A total of 300 blood samples were collected and divided into three groups: the first trimester (control = 50, PE = 50), second trimester (control = 50, PE = 50), and third trimester (control = 50, PE = 50) groups. Placentas were obtained from normal pregnancies (n = 20) and gestationally matched pregnancies complicated by early-onset PE (n = 20). All of them had undergone caesarean deliveries from Jan. 2021 to Dec. 2021 at the Department of Gynaecology and Obstetrics, the First Affiliated Hospital of Jinan University (Guangzhou, China). The PE diagnosis was based on the criteria issued by the International Society for the Study of Hypertension in Pregnancy (ISSHP) in 2018 [23]. The clinical data of the patients are presented in Supplementary Table 1. The criteria of inclusion and exclusion for tissue collection are listed in Supplementary Table 2. First-trimester placental tissues (6–12 weeks of gestation) were obtained from women undergoing elective pregnancy terminations. This study was approved by the Ethics Committee of the First Affiliated Hospital of Jinan University (approval number: KY-2021-092) and conducted in accordance with the Declaration of Helsinki. Signed informed consent was obtained from all the study participants.

### 2.2. Proteomics analysis

Placental tissues from patients with PE (n = 4) and normal pregnant women (n = 5) were used for proteomics analysis. The detailed method of proteomics identification has been previously described [24]. Finally, the R package MSstats was used to evaluate significant differences in protein expression, and the genes with fold change >1.5 and *p-value* < 0.05 were identified as differentially expressed proteins (DEPs). Cytoscape (a software for network biology analysis) was used for protein-protein interaction (PPI) network analysis of differentially expressed genes.

### 2.3. Animal model

Sprague-Dawley rats were purchased from Beijing Vital River Laboratory Animal Technology Co., Ltd. (SCXK 2012–0001, Beijing, China). Based on a previous report [25], we established a rat model of FTL knockdown by intravenously injecting FTL-targeted short hairpin (sh) RNA adenovirus (Ad-shFTL) and the control adenovirus (Ad-control) (OBiO Technology Co., Shanghai, China). Briefly, rats in the same batch were randomly assigned to the Ad-control (n = 10) and Ad-shFTL groups (n = 10). On gestation day (GD) 7.5, recombinant adenoviruses were injected intravenously via the tail vein at a dose of approximately $1–2 \times 10^9$ pfu per rat. After the adenovirus injection, ferrostatin-1 (Fer-1)--treated rats received intraperitoneal injections of either saline (control) or Fer-1 (2 μmol/kg body weight; catalogue #S7243, Selleck) every two days as previously described [26]. Pregnant rats were sacrificed to collect peripheral blood, fetal, kidney, and placental tissues on GD17.5. All the experimental processes involving animal treatments were conducted per the procedures of the Ethical Committee for Animal Experimentation, Jinan University (approval number: 20211029–010).

Measuring blood pressure and proteinuria as well as Doppler ultrasound evaluation was implemented as previously described [27,28]. The blood pressure of conscious pregnant rats was measured using an automated computerized tail-cuff system after five consecutive training periods (Visitech BP2000, Visitech Systems, Inc., USA). On GD16.5, the rats were individually housed in metabolic cages, and 24-h urine samples were collected for further analysis. The uterine artery pulsatility index (PI) and resistance index (RI) were measured via Doppler ultrasonography (Mylab 30CV, Esaote, Italy) at GD17.5 [14,29]. The levels of UA, AST, ALT, BUN, and CREA in the blood were analysed by an automatic biochemical analyser (HITACHI 7020, Tokyo, Japan).

### 2.4. Tissue explants, cell lines, and cell viability assay

In vitro culture of chorionic villous explants was performed as previously described [30]. The human trophoblast cell line HTR8/SVneo was purchased from Zhongqiao Xinzhou Biotechnology Co., Ltd. (Shanghai, China). HTR8/SVneo cells were all cultured at 37 °C under standard conditions. Short hairpin RNA (shRNA) targeting FTL and a scramble shRNA were purchased from OBiO Technology Co., Ltd. (Shanghai, China). The target sequences against human FTL and scrambled shRNA were cloned into the shuttle vector of an adenovirus packaging system as previously described [31]. All cells were cultured in 96-well plates ($2.5 \times 10^4$ cells/ml) as described above and were treated in the absence or presence of Fer-1 (5 μM), Z-VAD (10 μM), 3-MA (5 μM), or Necro (20 μM) for 36 h. Subsequently, 10 μl CCK-8 reagent was added to the wells of 96-well plates, and the cells were incubated for 3 h at 37 °C. The absorbance values were measured at 450 nm using a Bio-Rad Model 450 microplate reader (Bio-Rad, CA, USA).

### 2.5. Histological analysis

Haematoxylin and eosin (HE) staining was conducted according to routine protocols. Glycogen staining was performed using a Periodic Acid-Schiff (PAS) kit (Sigma-Aldrich) following the manufacturer's protocol. Immunofluorescence and immunohistochemical staining were performed as previously described [32]. Human or rat tissues were serially sectioned at thicknesses of 4 μm. Then, the sections were incubated with primary antibodies overnight at 4 °C. Subsequently, the sections were incubated with fluorescent secondary antibodies. The nuclei were stained with DAPI (Invitrogen). The sections were photographed using a fluorescence microscope (Olympus BX53, Tokyo, Japan). A minimum of five random images from three samples were analysed per group. Immunohistochemical statistical analysis was conducted with the optical density (OD). The details of the antibodies are listed in Supplementary Table 3.

### 2.6. Western blotting analysis

Western blotting experiments for identifying the proteins from various tissues and HTR-8/SVneo cells were performed with at least three replicates as described previously [33]. The details of the antibodies are listed in Supplementary Table 4.

### 2.7. Enzyme-linked immunosorbent assay (ELISA)

Whole blood samples were collected from human and rat maternal or umbilical cord blood. The substances to be tested in the sera were measured by UV spectrophotometry using detection kits according to the manufacturer's instructions (Mbbiology Biological, Jiangsu, China). The details of the kits are listed in Supplementary Table 5.

### 2.8. Transmission electron microscopy (TEM)

Biopsies from rat kidneys (1 $mm^3$) were fixed for 2–4 h at 4 °C, washed, and stored overnight at 37 °C. The fixed samples were then prepared for ultrathin sectioning. After uranium–lead double staining, the samples were incubated at room temperature overnight, and images were collected and analysed under a transmission electron microscope (HT7700, Hitachi, Japan). The mitochondrial morphology of HTR-8/SVneo cells was observed by TEM as previously reported [34].

### 2.9. Flow cytometry

Apoptotic rates in transfected HTR8/SVneo cells were evaluated using the FITC-Annexin V Apoptosis Detection Kit (Beyotime Institute of Biotechnology, Shanghai, China) by FACS Caliber flow cytometry (Becton Dickinson, CA, USA) according to the manufacturer's instructions. Transfected HTR8/SVneo cells were washed with PBS three times and stained with Annexin V-FITC and propidium iodide (PI) for 20 min at room temperature. Then, the apoptotic cells were counted with flow cytometry and analysed using WinMDI software (The Scripps Research Institute, CA, USA).

### 2.10. Transwell migration and invasion assay

Transfected cells ($1 \times 10^5$ HTR-8/SVneo cells in 100 μl serum-free medium) were seeded into transwell inserts (8-μm pores; #3422, Costar, Cambridge, MA), and the rest of the protocol was introduced in a previous report [35]. According to previously reported methods, cell migration was detected by scratch assay [36]. The images of migrated cells were recorded at 0–48 h. The percentage of wound closure was analysed.

### 2.11. RNA sequencing analysis

Whole-genome gene expression analysis was performed in HTR8/SVneo cells from the shNC group (n = 3) and shFTL group (n = 3). Total RNA was extracted using TRIzol, and cDNA samples were sequenced using a HiSeq3000 sequencing system (Illumina). Transcriptome sequencing experiments were performed by Tsingke Biotechnology Co., Ltd. (Beijing, China).

### 2.12. Lipid peroxidation assay

Detection of cells and tissue lipid peroxidation signatures, such as GSH (Sigma-Aldrich, St. Louis, MO, USA), GPX (ab102530; Abcam), MDA (WEIAO BioTech), and total and labile $Fe^{2+}$ contents (Iron Colorimetric Assay Kit, Cat: 8448) were measured according to the manufacturer's instructions.

Intracellular ROS were quantitatively measured using a DCFH-DA red fluorescent probe as previously reported [36]. For quantitative analysis, the ROS levels were detected by flow cytometry (NovoCyte 2060R; ACEA Bioscience, Inc.) and analysed using FlowJo v10 (FlowJo, LLC).

Mitochondrial membrane potential was detected using the JC-1 Mitochondrial Membrane Potential Assay Kit (Abcam) following the manufacturer's instructions. For quantitative analysis, flow cytometry analysis was performed to assess the mitochondrial membrane potential as previously described [37].

### 2.13. Statistics

Statistical analysis was performed using SPSS 26.0 software (IBM SPSS 26.0, SPSS Inc.). The construction of statistical charts was performed using the GraphPad Prism 8 software package (GraphPad Software, CA, USA). A *t*-test was used to analyse the normally distributed continuous variables, and the Mann–Whitney *U* test was used to analyse the nonnormally distributed data. All values are presented as the mean ± SD or median (interquartile range). $P < 0.05$ was considered statistically significant.

## 3. Results

### 3.1. FTL, expressed in trophoblast cells, was significantly reduced in the serum and chorionic villi of patients with PE

The component analysis of proteomics based on the placental tissues from five healthy pregnant women and four pregnant women with PE showed the differentially expressed genes (Fig. 1A and B). The demographic data of the study population have been previously described in detail [24]. According to the CytoHubba plug-in MCC algorithm in Cytoscape software, the top three proteins with high core degrees were analysed (Fig. 1C). Our results showed that the expression levels of FTL

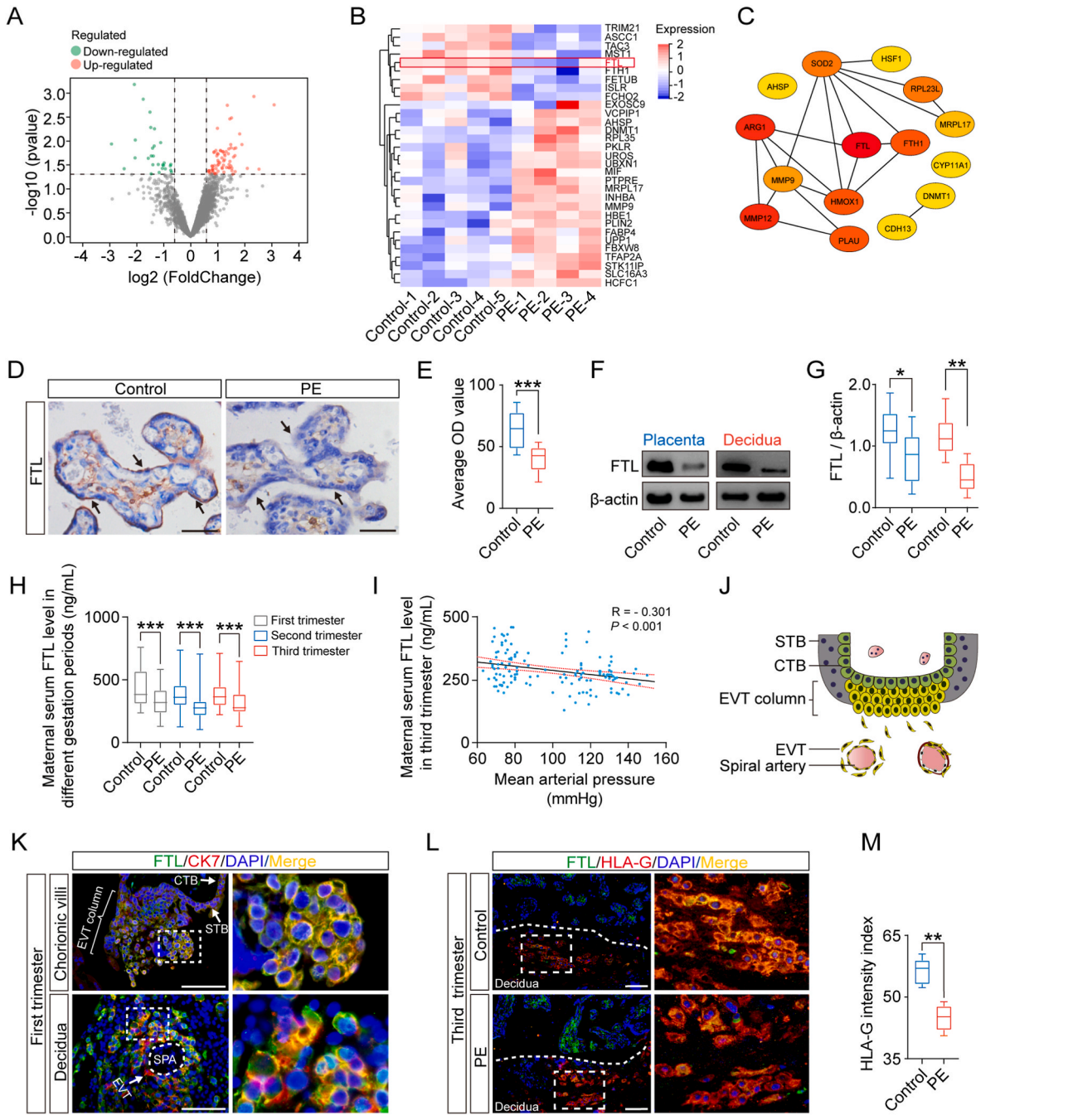


**Fig. 1.** Examining FTL levels in maternal serum and placenta of control and patients with PE.
**A**: Volcano plot (significance vs. fold change) of differentially expressed genes (fold change ≥1.5 and $p$-value < 0.05) in placental tissue between control and PE patients. **B**: Heatmap showing the top 31 differentially expressed genes in the placental tissues from five control and four PE patient samples. **C**: A protein-protein interaction (PPI) network of differentially expressed genes was constructed using Cytoscape software. **D-E**: FTL immunohistochemical staining of transverse sections of placental chorionic villi (D) and the optical density (OD)-based relevant quantification (E) from the control and PE groups. **F-G**: Western blot showing FTL expression (F) and quantification analysis of expression levels (G) from the control and PE groups. **H–I**: ELISA data showing maternal serum FTL levels during pregnancy from the control and PE groups (H), and Pearson correlation analysis was conducted to show the correlation between FTL levels during pregnancy and mean arterial blood pressure (MAP) (I). **J**: Schematic representation of placental anchoring villus on maternal decidua. **K**: Immunofluorescence showing colocalization of FTL (green) and CK7 (red) in first-trimester chorionic villus and decidual tissue. **L-M**: Immunofluorescence showing colocalization of FTL (green) and HLA-G (red) in third-trimester decidual tissue (L) and the immunofluorescence intensity-based relevant quantification (M) from the control and PE groups. Scale bars = 100 μm in D, K, and L. *$P$ < 0.05; **$P$ < 0.01; ***$P$ < 0.001. . (For interpretation of the references to color in this figure legend, the reader is referred to the Web version of this article.)

and FTH1 were reduced in preeclamptic placentas, while Western blot analysis showed that there was no significant difference in the expression of ARG1. Meanwhile, FTH1 was mainly expressed in the placental villous stroma rather than trophoblasts (Supplementary Figs. 1A–C). Therefore, FTL was proposed as a key molecule for the current research. Next, FTL immunocytochemistry and Western blotting were used to detect the expression changes of FTL in both human placental and decidual tissues of healthy pregnant women and patients with PE (note:

their demographic information is shown in Supplementary Table 1) (Fig. 1D–G). ELISA was conducted to determine serum FTL levels in healthy pregnant women and PE patients at different gestational periods, including the first, secondary, and third trimesters (note: their demographic information is shown in Supplementary Table 1) (Fig. 1H). The correlation analysis also demonstrated the inverse relationship between serum FTL levels in late gestation and maternal mean arterial pressure (Fig. 1I). Based on the dominant theory about PE pathogenesis, i.e., inadequate remodelling of the uterine spiral artery (Fig. 1J), we confirmed that FTL was expressed in earlier cytotrophoblasts and subsequent EVTs using co-immunofluorescence of FTL and cytokeratin 7 (CK7) in cross-sections of chorionic villi and decidua (Fig. 1K), as well as the reduced FTL expression in EVTs using co-immunofluorescence of FTL and human leukocyte antigen-G (HLA-G) (Fig. 1L-M), implying inadequate remodelling of the uterine spiral artery in PE patients (Supplementary Figs. 1D–F).

### 3.2. The phenotypes of patients with PE were perfectly mimicked in the FTL downregulating rat model

A rat model of FTL downregulation was established by intravenously injecting adenoviruses expressing shRNA targeting FTL (Ad-shFTL) into the rat tail vein (Fig. 2A) as previously described [38]. First, the downregulation efficiency of FTL expression was verified in HTR-8/SVneo cells and rat placentas (Supplementary Figs. 2A–F). In the FTL-downregulated pregnant rats, intravenously injecting adenoviruses expressing shRNA targeting FTL significantly increased both systolic blood pressure (SBP) and diastolic blood pressure (DBP) (Fig. 2B), as well as 24-h proteinuria (Fig. 2C), for at least one week. H&E and PAS staining manifested morphological damage in the glomerulus (e.g., narrower Bowman's capsule); TEM images of the rat glomerulus indicated ultrastructural damage to the glomerulus (e.g., podocyte oedema, collapsed vascular lumen, endothelial hyperplasia) (Fig. 2D and E); Doppler sonography showed an increased uterine artery PI value

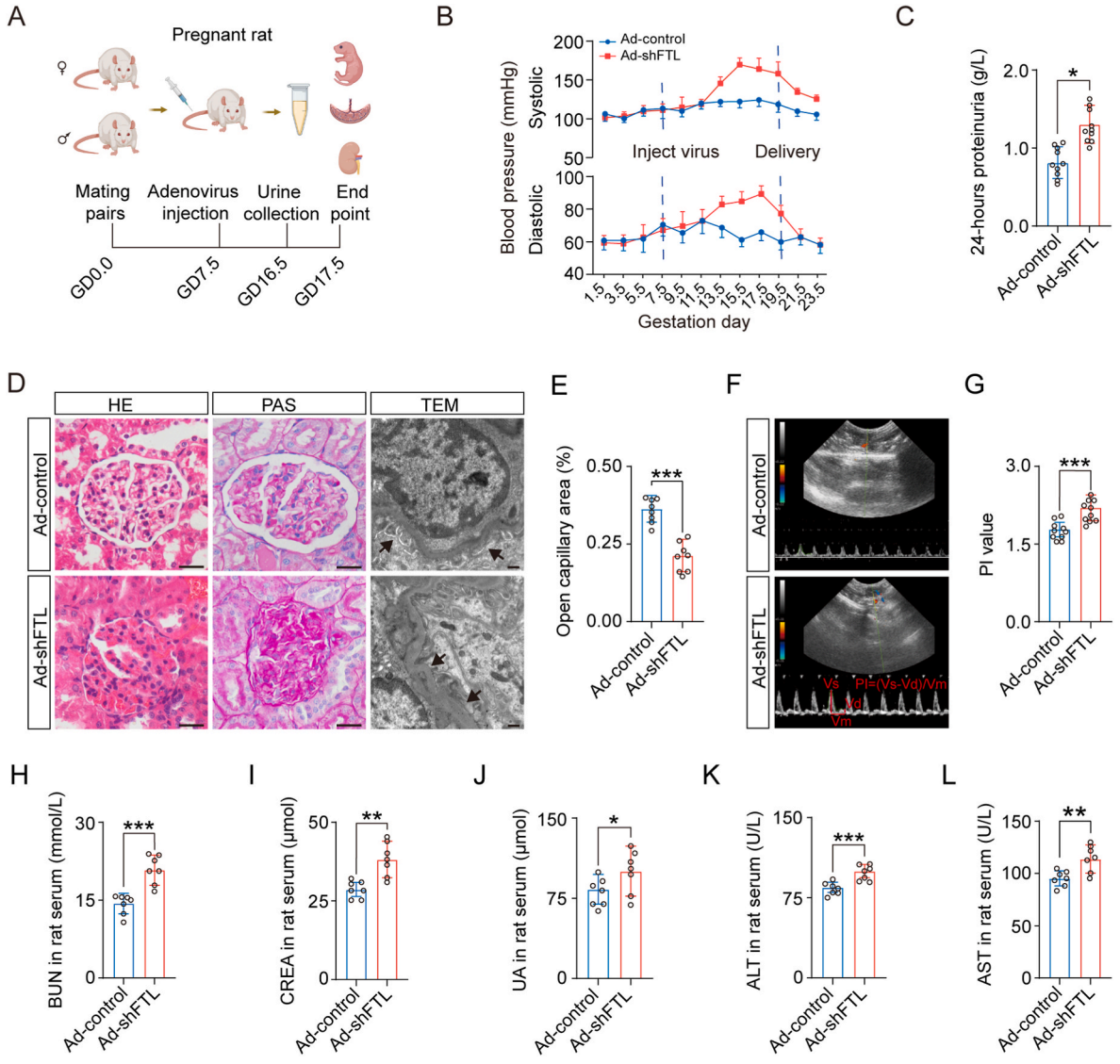


**Fig. 2.** Assessing a pregnant rat model of FTL knockdown by intravenously injecting a recombinant adenoviral shRNA vector.
**A**: Schematic illustration of the establishment of a downregulated FTL-pregnant rat model. **B**: The systolic and diastolic pressure from the Ad-control and Ad-shFTL groups. **C**: The 24-h proteinuria from the Ad-control and Ad-shFTL groups. **D-E**: Representative images of glomeruli stained with HE and PAS, as well as TEM (D), and the comparison of open capillary areas between the Ad-control and Ad-shFTL groups (E). **F-G**: Representative ultrasonography of rat uterine arteries (F), and the bar charts show the PI value (G) from the Ad-control and Ad-shFTL groups. **H-L**: The levels of blood urea nitrogen (BUN) (H), creatinine (CREA) (I), uric acid (UA) (J), alanine aminotransferase (ALT) (K), and aspartate aminotransferase (AST) (L) in rat serum of the Ad-control and Ad-shFTL groups. Scale bars = 100 μm in light microscopy of D; 2 μm in electronic microscopy of D. $^{*}P < 0.05$; $^{**}P < 0.01$; $^{***}P < 0.001$.

(Fig. 2F and G); biochemical tests demonstrated significant increases in BUN, CREA, UA, ALT, and AST in rat serum (Fig. 2H-L) in the FTL downregulation group. In addition, fetal growth restriction and placental abnormalities were also observed in the FTL-downregulated pregnant rats (Supplementary Figs. 3A–I). In contrast, there were no significant changes in blood pressure, 24-h proteinuria, or glomerular morphology in nonpregnant rats following intravenous injection of adenoviruses expressing shRNA targeting FTL (Supplementary Figs. 4A–E). This data certainly suggested that the pregnant rat model of FTL downregulation showed the same phenotypic traits as the clinical manifestations in patients with PE.

### 3.3. FTL downregulation caused defective uterine spiral artery remodelling in a rat model

CK7 immunocytochemistry was implemented on cross-sections of the placenta to determine the invasion of trophoblasts into the uterine wall as previously reported [39], and the results showed weaker interstitial trophoblast invasion, which is reflected by the surface area invaded by trophoblast cells in the mesometrial triangle (i.e., the maximal distance into the width and depth), in the FTL downregulation group (Fig. 3A–C). Meanwhile, based on the classifications of the uterine spiral artery remodelling [39] (Fig. 3D), uterine spiral artery remodelling was divided into four categories (i.e., Cat. 1–4) in different zones (i.e., Zones 1–3) (Fig. 3E). The analysis results demonstrated that a significant difference in uterine spiral arteries between the control and shFTL groups in zone 1 and zone 3 was found in Cat. 1, Cat. 2, and Cat. 4; there were no significant differences in Cat. 3. Three remodelled uterine spiral arteries in zone 1 and zone 3 (Fig. 3F–I). Meanwhile, the analysis results demonstrated that the significant difference in remodelled uterine spiral arteries between the control and shFTL groups in total zones was Cat. 1 and Cat. 4 (Supplementary Fig. 5A); there were significant differences in Cat. 1 remodelled uterine spiral arteries in all zones; there were significant differences in Cat. 2 and Cat. 4 remodelled uterine spiral arteries in zone 1 only between the control and shFTL groups (Supplementary Figs. 5B–D). Co-immunofluorescence of CK7 and α-SMA showed the unremodelled uterine spiral arteries in the shFTL group (Fig. 3J), which was strengthened by quantitative analysis, including the luminal area of the spiral artery (Fig. 3K), mean α-SMA intensity on the smooth muscle of spiral artery (Fig. 3L), and mean CK7 fluorescent intensity in EVTs (Fig. 3M).

### 3.4. Blocking ferroptosis successfully reversed the defective uterine spiral artery remodelling and PE symptoms in the FTL-downregulated rat model

To prove the importance of FTL downregulation-induced ferroptosis, we simultaneously injected Fer-1 and shFTL adenoviruses intravenously into pregnant rats (Fig. 4A). Western blot data showed that blocking ferroptosis with Fer-1 reversed shFTL-induced decreases in GPX4, SLC7A11, and FTH1 expression as well as increase in ACSL4 expression (Fig. 4B). Meanwhile, lipid peroxidation results showed that blocking ferroptosis with Fer-1 reversed shFTL-induced reductions in GSH concentration and GPX activity, as well as increases in $Fe^{2+}$ and MDA concentrations (Fig. 4C–F). Co-immunofluorescence of CK7 and α-SMA on the cross-sections of decidua showed that blocking ferroptosis with Fer-1 was able to rescue the shFTL-induced increase in unremodelled uterine spiral arteries (Fig. 4G–I). HE and PAS staining and TEM showed that blocking ferroptosis with Fer-1 could rescue shFTL-induced morphological damage in the glomerulus (e.g., narrower Bowman's capsule) and ultrastructural damage to the glomerulus (e.g., podocyte oedema, collapsed vascular lumen, endothelial hyperplasia) (Fig. 4J and K), as well as 24-h proteinuria and rat blood pressure (Fig. 4L and M). Additionally, we also found other reverse actions of shFTL-induced PE indices, including fetal growth restriction, placental abnormality, uterine artery PI value, and kidney function indicators (Supplementary Fig. 6A-P). It is suggested that blocking ferroptosis could indeed rescue FTL downregulation-induced PE-like phenotypes by reversing defective uterine spiral artery remodelling.

### 3.5. Ferroptosis is the main cause of defective uterine spiral artery remodelling induced by FTL downregulation

According to the trajectory of trophoblasts during the uterine spiral artery (Fig. 5A), we checked whether FTL downregulation affected epithelial-mesenchymal transition (EMT), migration/invasion, and cell death. In the context of FTL downregulation, Western blotting showed a reduction in N-cadherin and vimentin but no changes in E-cadherin in HTR-8/SVneo cells (Fig. 5B–E). Transwell, scratch test, and chorionic villous explant culture assays demonstrated inhibited HTR-8/SVneo or trophoblast cell invasion/migration (Fig. 5F–K). Propidium iodide (PI) immunofluorescence and flow cytometry revealed a significant increase in trophoblast cell death (Fig. 5L-N).

This data suggest that the death of trophoblast cells caused by FTL downregulation may play an important role in defective uterine spiral artery remodelling. This speculation derived from the above experimental observations was verified by the prediction of relevant signalling pathways based on RNA sequencing in HTR-8/SVneo cells with downregulated FTL (Fig. 6A–C). Furthermore, the addition of ferrostatin-1 (Fer-1), a selective inhibitor of ferroptosis, obviously reversed the shFTL-induced decrease in cell viability (Fig. 6D) and the shFTL-induced changes in most ferroptotic marker concentrations/activities (Fig. 6E–H) in FTL-downregulated HTR-8/SVneo cells, which were momentously confirmed by the expression changes in ACSL4, GPX4, SLC7A11, and FTH1 in the context of FTL downregulation using Western blot and corresponding assay kits (Fig. 6I and J, Supplementary Figs. 7A–F). Likewise, co-immunofluorescence of calcein-AM and DCFH-DA showed the reversals of shFTL-induced increases in intracellular free iron levels and ROS after treatment with Fer-1 (Fig. 6K-M); JC-1 staining showed that Fer-1 addition could efficiently reverse the change in mitochondrial membrane potential in FTL-downregulated HTR-8/SVneo cells (Fig. 6N-O); TEM showed the apparent recovery of shFTL-induced mitochondrial collapse in the presence of Fer-1 in HTR-8/SVneo cells (Fig. 6P). Blocking ferroptosis with Fer-1 could also effectively reverse the reduction in invasion and migration, as well as PI-immunofluorescently labelled HTR-8/SVneo cell death, as revealed by transwell, scratch test, and chorionic villous explant culture assays (Supplementary Figs. 8A–G).

### 3.6. Ferroptosis occurs in the placental tissues of patients with PE

Our results showed a reduction in GSH concentration and GPX activity and an increase in $Fe^{2+}$ concentration and MDA concentration in the placental tissues of PE patients (Fig. 7A–D). Western blot analysis demonstrated increased expression of ACSL4 and decreased expression of GPX4 in the placental tissues of PE patients (Fig. 7E). Likewise, immunocytochemistry data showed the same trend in gene expression change of ACSL4 and GPX4 in the chorionic villi of PE patients as in Western blot (Fig. 7F and G). Finally, clinical correlation analysis indicated that there were adverse relationships between maternal mean arterial pressure and GSH concentration or GPX activity and a positive relationship between maternal mean arterial pressure and $Fe^{2+}$ or MDA concentration (Fig. 7H–K). Furthermore, we found that there was a significant positive correlation between maternal FTL level and GSH concentration or GPX activity and an adverse relationship between maternal FTL level and $Fe^{2+}$ concentration or MDA concentration (Fig. 7L-O). This suggests that ferroptosis plays an important role in FTL downregulation-induced pathogenesis of PE.

## 4. Discussion

In this study, we found FTL in the process of screening differentially expressed genes in PE patient sampling using a proteomics approach

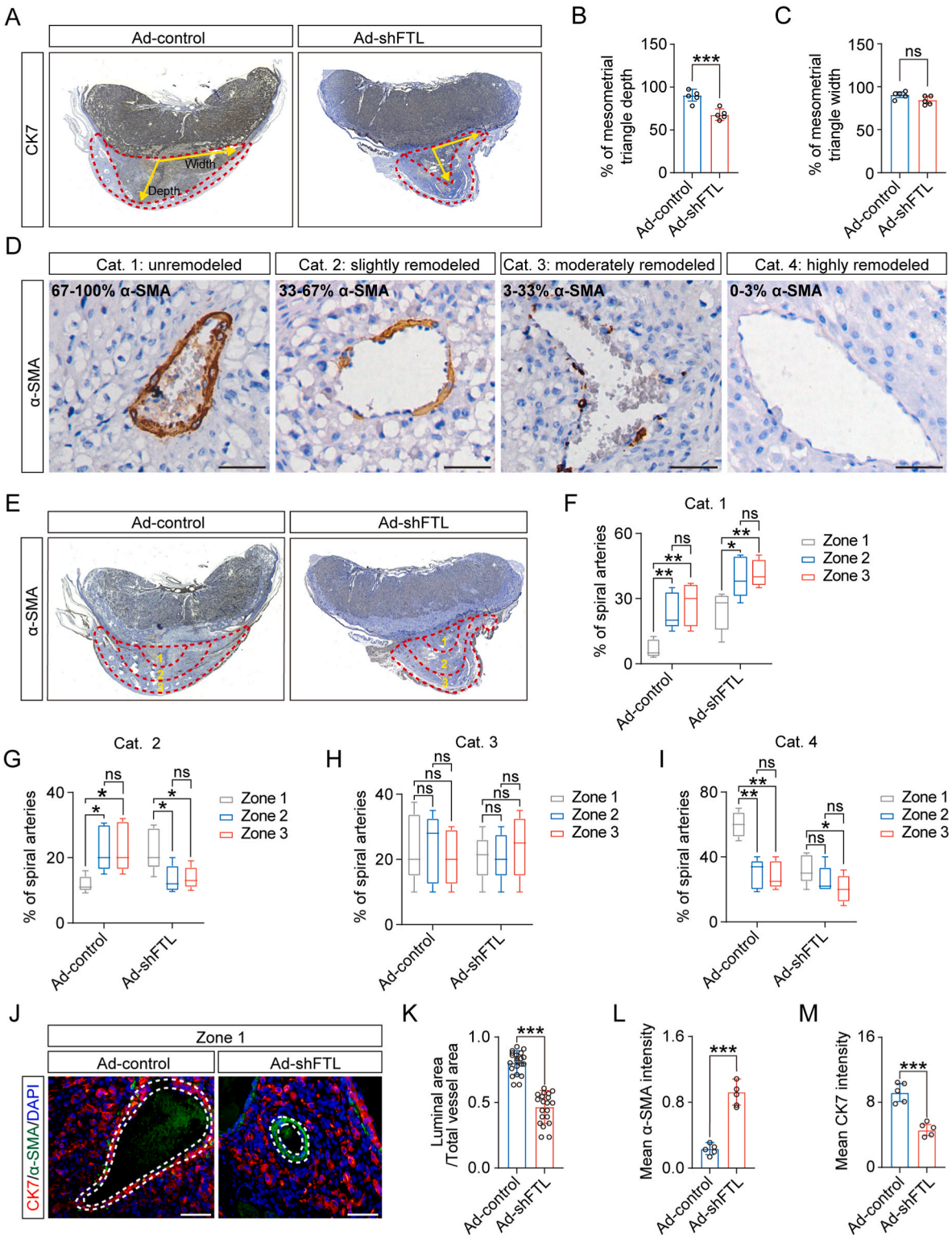


**Fig. 3.** Evaluating uterine spiral artery remodelling in different aspects of rat placenta.
**A**: Mesometrial triangle immunochemically stained with CK7 acts as the evaluation criteria to measure invasion depth and width. **B–C**: Comparisons of the depths (B) and width (C) between control and FTL knockdown pregnant rats. **D**: Mesometrial triangle immunochemically stained with α-SMA was divided into the three consecutive zones of equal width to provide the partition criterion in the following four categories (cat). Briefly, unremodelled arteries with 67–100% a-SMA staining (cat. 1), slightly remodelled arteries with 33–67% a-SMA staining (cat. 2), moderately remodelled arteries with 3–33% a-SMA staining (cat. 3) and highly remodelled arteries with 0–3% a-SMA staining in the arterial wall (cat. **E-I**: Statistics on the distribution of four categories of spiral arteries in three regions from control and FTL knockdown pregnant rats. **J-M**: Representative images of CK7 and α-SMA immunofluorescence staining in the cross-sections of decidua basalis of control and FTL-knockdown pregnant rats (J), and the bar charts showing the ratios of luminal area to total vessel area (K) and fluorescence intensity of α-SMA and CK7 in zone 1 (L–M) from control and FTL-knockdown pregnant rats. Scale bars = 100 μm in D and J. *$P < 0.05$; **$P < 0.01$; ***$P < 0.001$; ns = no significance.

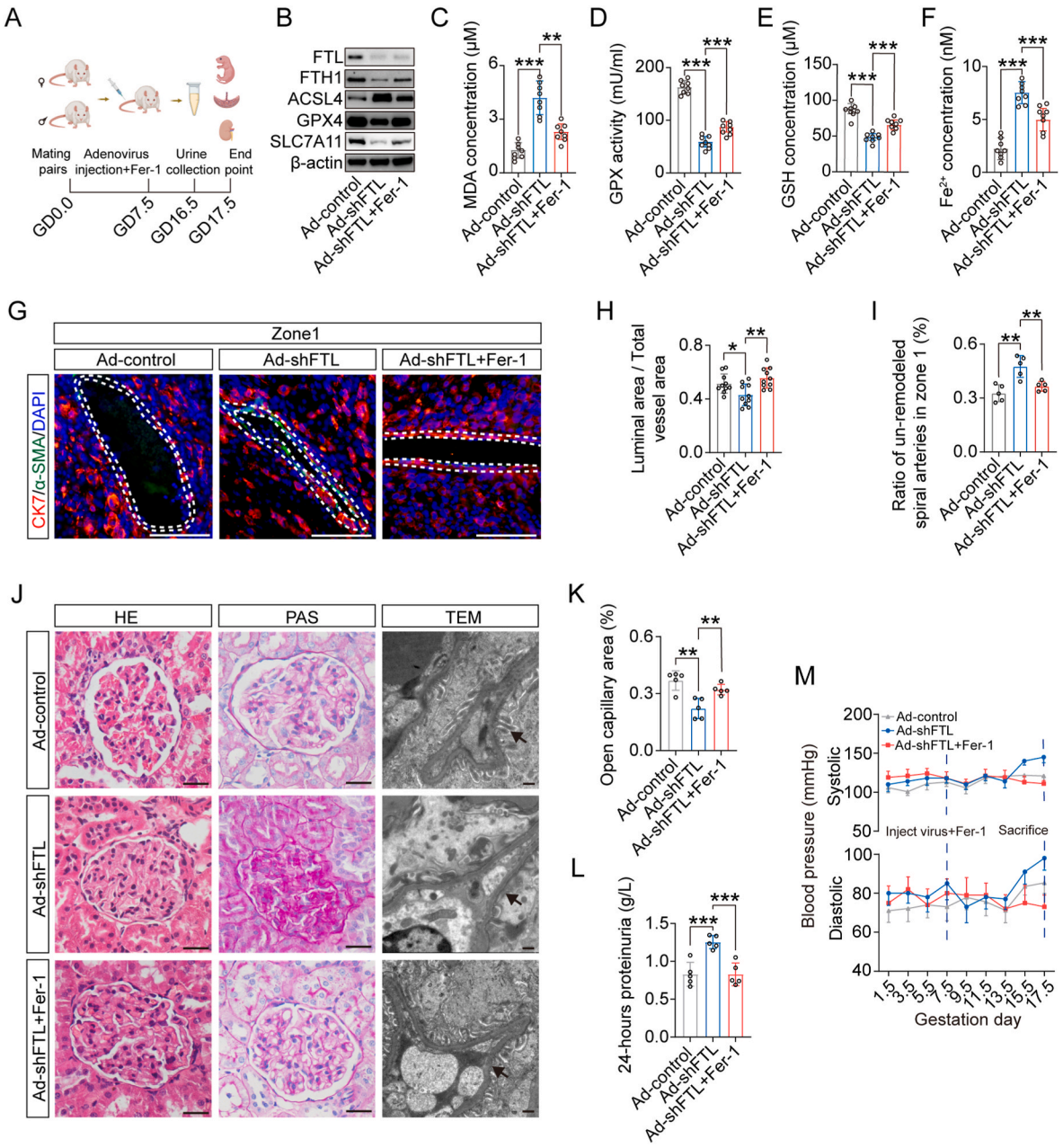


**Fig. 4.** Assessing the PE indicators in a pregnant rat model of FTL knockdown and pharmacological blockade of ferroptosis.
**A**: Schematic illustration showing that ferroptosis is blocked in a pregnant rat model of FTL knockdown. **B**: Western blot data showing the expression of ACSL4, GPX4, SLC7A11, and FTH1 in rat placentas. **C–F**: Lipid peroxidation and iron colorimetric assays were used to detect MDA concentration (C), GPX activity (D), GSH concentration (E), and $Fe^{2+}$ concentration (F) in the Ad-control, Ad-shFTL, and Ad-shFTL + Fer-1 groups. **G-I**: Representative images of CK7 and α-SMA immunofluorescence staining in the cross-sections of rat decidua basalis of FTL knockdown and pharmacologically blocking ferroptosis with ferroptosis inhibitor (G), and the bar charts showing the ratios of the luminal area to total vessel area (H) and the ratio of unremodelled spiral arteries in zone 1 (I) from Ad-control, Ad-shFTL, and Ad-shFTL + Fer-1 groups. **J-K**: Representative images of glomeruli stained with HE, PAS, and TEM (J) and the comparison of open capillary areas from the Ad-control, Ad-shFTL, and Ad-shFTL + Fer-1 groups (K). **L-M**: The 24-h proteinuria (L) and systolic and diastolic pressure (M) from the Ad-control, Ad-shFTL and Ad-shFTL + Fer-1 groups. Scale bars = 100 μm in G and light microscopy of J; 2 μm in electronic microscopy of J. $^{*}P < 0.05$; $^{**}P < 0.01$; $^{***}P < 0.001$.

based on the updated database (Fig. 1). Of course, it might just be a coincidence between the low FTL level and PE development during pregnancy if simply relying on the above clinical bioinformatic analysis. The causal relationship between them was substantiated when PE-like phenotypes (i.e., increases in systolic and diastolic pressure, 24-h proteinuria, liver and kidney damage, fetal growth restriction, and placental abnormalities) were observed in pregnant rats, in which FTL expression was downregulated by intravenously injecting adenoviruses expressing shRNA targeting FTL (Fig. 2, Supplementary Fig. 3). Thus, we focused heavily on investigating how FTL was involved in PE pathogenesis in follow-up studies.

Although the aetiology of PE is still obscure, growing evidence has shown that PE is allied to an abnormal inflammatory response at the maternal-fetal interface, which in turn induces deficient uterine spiral artery remodelling, i.e., a generally accepted hypothesis in the pathophysiology of PE [40]. Since FTL is expressed in fetal-derived trophoblasts (Fig. 1), it came naturally to us that FTL might be involved in uterine spiral artery remodelling by regulating trophoblast/EVT invasion. The results of the analysis indicated that deficiency of FTL caused inadequate uterine spiral artery remodelling in the pregnant rats;

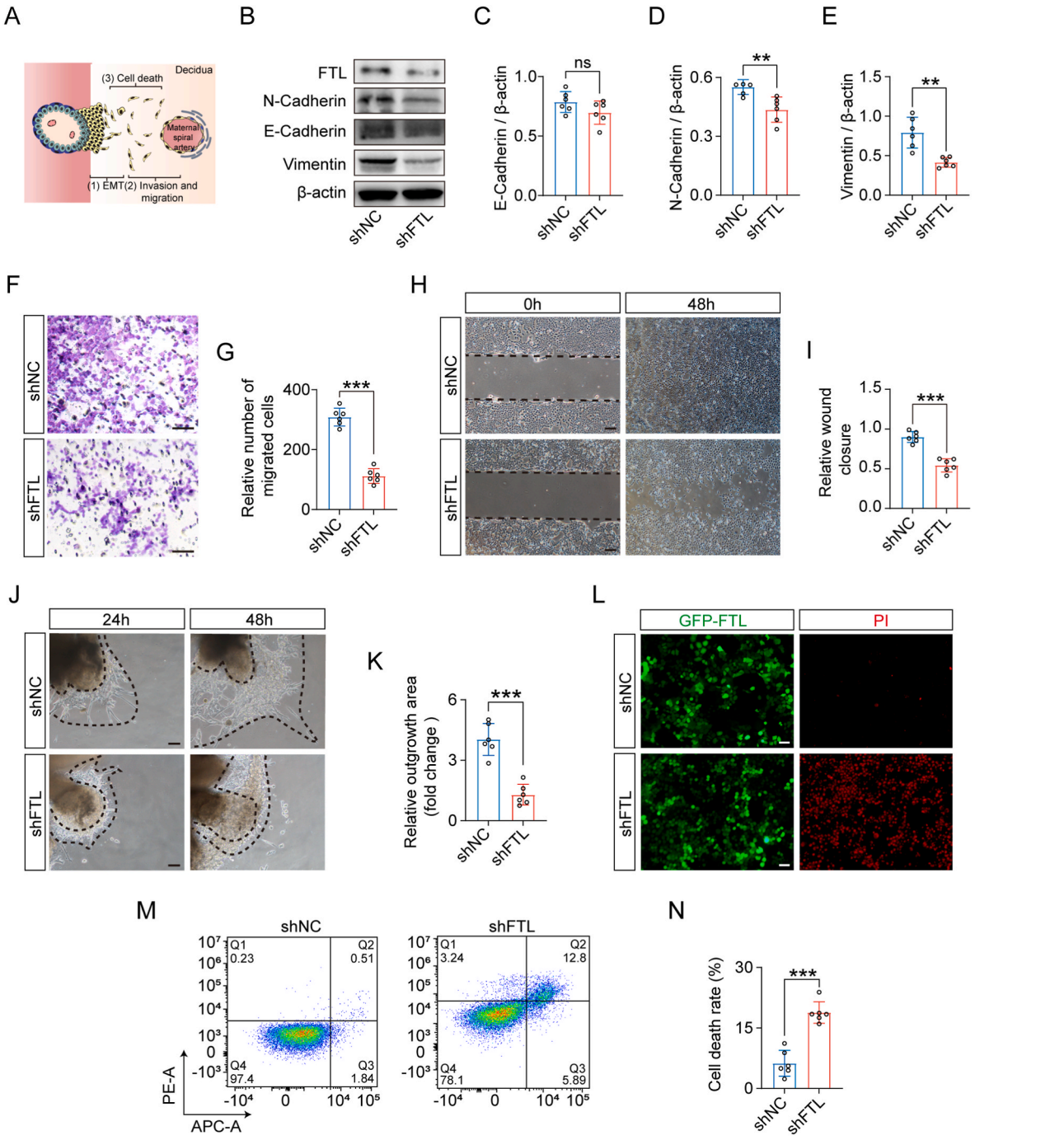


**Fig. 5.** Assessing the migration/invasion and cell death in FTL-knockdown HTR-8/SVneo cells and chorionic villous explants.
**A**: Schematic illustration of the process of spiral artery remodelling. **B-E**: Western blot data showing the expression of FTL, N-cadherin, E-cadherin, and vimentin (B), and the bar charts indicate the quantitative analysis of E-cadherin (C), N-cadherin (D), and vimentin (E) in HTR-8/SVneo cells from the control and shFTL groups. **F-G**: Representative images of the transwell assay of HTR-8/SVneo cells (F), and the bar chart shows the relative numbers of migrated cells (G) from the control and shFTL groups. **H–I**: Representative images of wound healing assays of HTR-8/SVneo cells (H), and the bar charts showing relative wound closure (I) from the control and shFTL groups. **J-K**: Representative images of Matrigel-imbedded chorionic villous explant cultures (J) and the bar chart showing relative outgrowth areas (K) from the control and shFTL groups. **L**: Representative images of propidium iodide (PI) staining of HTR-8/SVneo cells from the control and shFTL groups. **M-N**: Cell death was measured by flow cytometry labelled with Annexin V-FITC and PI staining (M), and the bar chart shows the quantitative analysis of cell death rates from the control and shFTL groups (N). Scale bars = 100 μm in F, H, J, and L. $^{*}P < 0.05$; $^{**}P < 0.01$; $^{***}P < 0.001$; ns = no significance.

interestingly, the proportions of the remodelled spiral arteries decreased with increasing distance from the starting point of migratory EVT (Fig. 3, Supplementary Fig. 5). This implies that the poor trophoblast cell/EVT invasion/migration might not be able to reach and remodel the uterine spiral arteries far away from chorionic villi, thereby eventually reducing the total numbers of well-remodelled spiral arteries. This is to say that some key events in spiral artery remodelling were affected by the deficiency of FTL in trophoblast/EVTs. Many regulators, such as ferritin light chain (FTL), GPX4, nuclear factor erythroid 2-related Factor 2 (Nrf2), haem oxygenase-1 (HO-1), and nuclear receptor coactivator 4 (NCOA4), have been identified as being involved in regulating ferroptosis. To further verify the principal effect of FTL

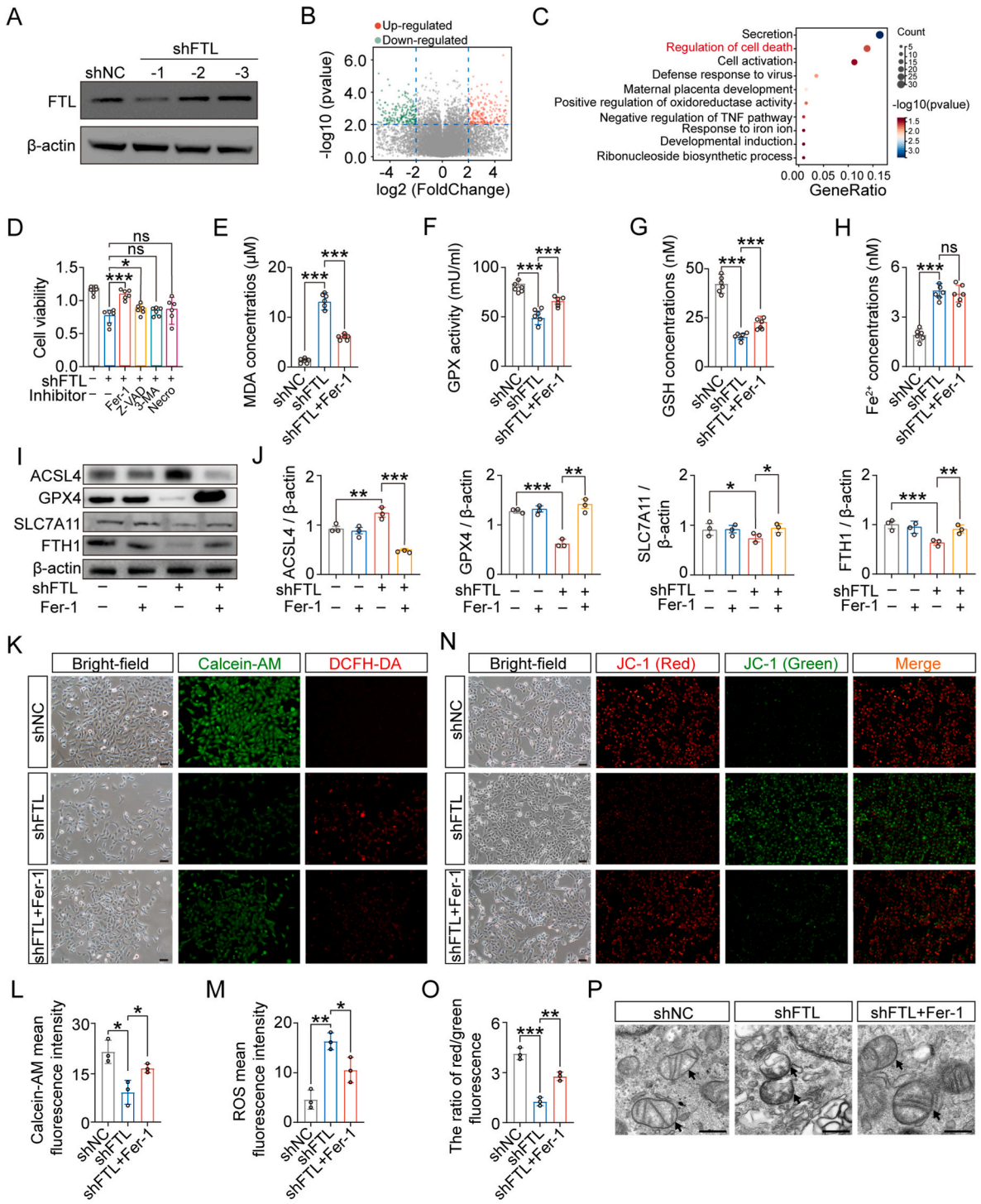


**Fig. 6.** Assessing the cell death in HTR-8/SVneo cells following the downregulation of FTL.
**A**: FTL expression determined by Western blot analysis in HTR-8/SVneo cells transfected with shNC, shFTL-1, shFTL-2 or shFTL-3. **B–C**: Volcano plot (significance vs. fold change) of differentially expressed genes (fold change ≥4 and $p$ value < 0.01) (B) and KEGG pathway (C) enrichment analysis of these differentially expressed genes. **D**: The measurement of HTR-8/SVneo cell viability with a cell counting kit-8 (CCK-8) from the control and shFTL with various inhibitors of cell death groups. **E-H**: Lipid peroxidation and iron colorimetric assays were used to detect MDA concentration (E), GPX activity (F), GSH concentration (G), and $Fe^{2+}$ concentration (H) in HTR-8/SVneo cells from the control, shFTL and shFTL + Fer-1 groups. **I-J**: Western blot data showing the expression of ACSL4, GPX4, SLC7A11, and FTH1 in HTR-8/SVneo cells in the absence or presence of FTL downregulation and blockade of ferroptosis (I), and the bar charts indicate the quantitative analysis of the expression of these genes (J). **K-M**: Representative bright-field and immunofluorescent (calcein-AM and DCFH-DA) images from the three groups (K), and the bar charts indicate the quantitative analysis of calcein-AM (L) and ROS (M) mean fluorescent intensity. **N–O**: Representative bright-field and immunofluorescent (JC-1) images from the aforementioned three groups (N), and the bar charts indicate the quantitative analysis of the ratio of red/green fluorescent intensity (O). **P**: Representative TEM images from the three groups. Scale bars = 50 μm in K and N; 2 μm in P. *$P$ < 0.05; **$P$ < 0.01; ***$P$ < 0.001; ns = no significance. . (For interpretation of the references to color in this figure legend, the reader is referred to the Web version of this article.)

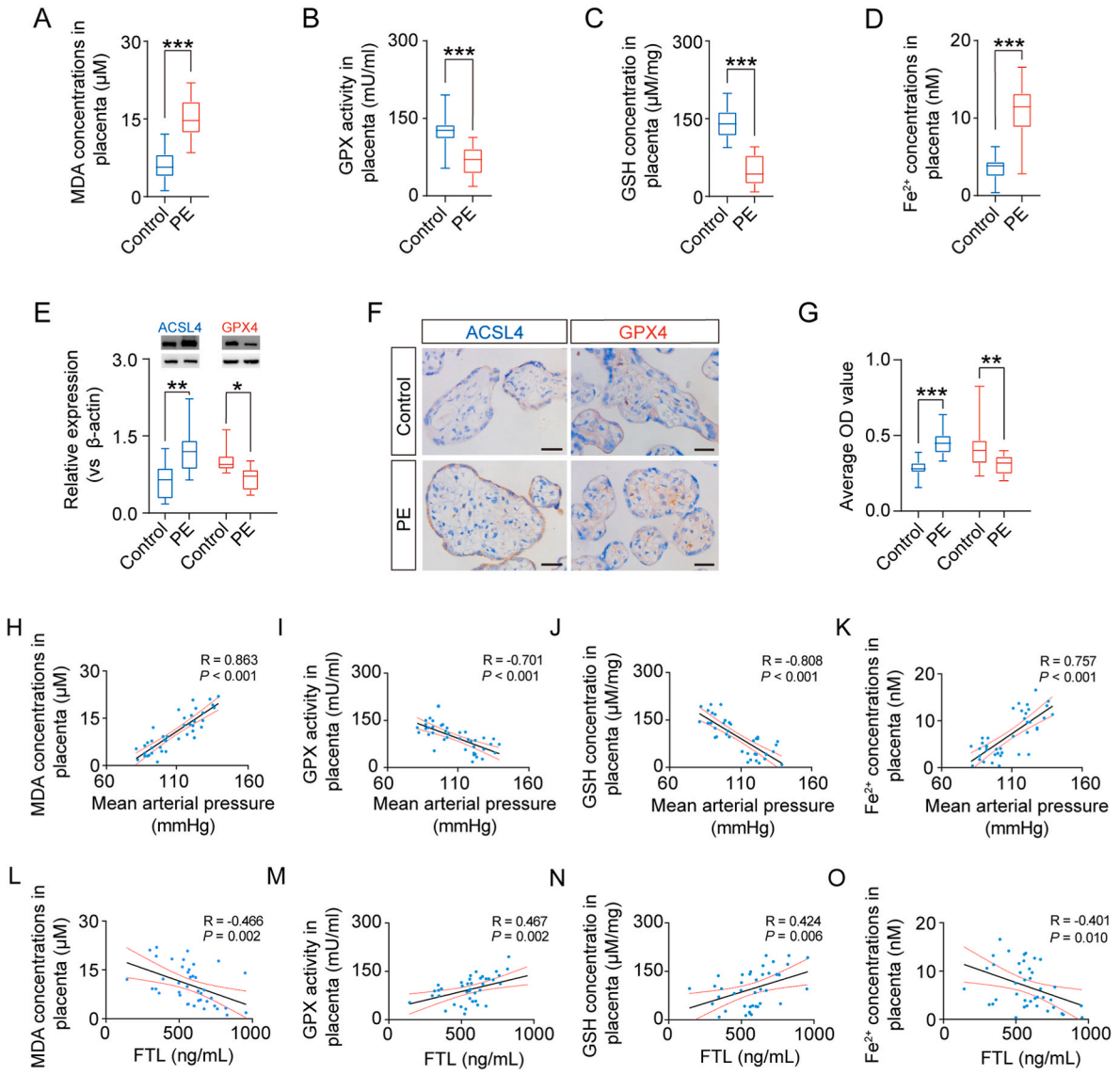


**Fig. 7.** Evaluation of ferroptosis in the placentas of patients with PE.
**A-D**: Lipid peroxidation and iron colorimetric assays were used to detect MDA concentration (A), GPX activity (B), GSH concentration (C), and $Fe^{2+}$ concentration (D) in the control and PE groups. **E**: Western blot data showing the expression of ACSL4 and GPX4 in human placental tissues. The bar chart indicates the quantitative analysis of ACSL4 and GPX4 expression in the control and PE groups. **F-G**: Immunocytochemical staining of cross-sections of human placental villi showing the expression of ACSL4 and GPX4 in human placental tissues (F). The bar charts indicate the quantitative analysis of relative expression and average OD values for GPX4 and ACSL4 from the control and PE groups (G). **H–K**: Correlation analysis was implemented between mean arterial pressure (MAP) and MDA (H), GPX (I), GSH concentration (J), and $Fe^{2+}$ concentration (K) in the placental tissues of patients. **L-O**: Correlation analysis was implemented between the FTL level and MDA (L), GPX (M), GSH concentration (N), and $Fe^{2+}$ concentration (O) in the placental tissues of patients. Scale bar = 100 μm in F. $^{*}P < 0.05$; $^{**}P < 0.01$; $^{***}P < 0.001$.

deficiency-induced ferroptosis, we checked whether blocking ferroptosis could alleviate or reverse deficient spiral artery remodelling and PE-like phenotypes in pregnant rats with FTL knockdown. From the perspective of the experimental results in pregnant rats with FTL knockdown (Fig. 4), we found that blocking ferroptosis with Fer-1 dramatically improved shFTL downregulation-induced excess lipid peroxidation, high $Fe^{2+}$ concentrations, and defective physiological changes in the spiral arteries, as well as a series of PE-like phenotypes (i.e., increases in systolic and diastolic pressure, 24-h proteinuria, liver and kidney damage, fetal growth restriction, and placental abnormalities) in pregnant rats with FTL knockdown (Fig. 4, Supplementary Fig. 6). We assumed that FTL deficiency-induced ferroptosis in trophoblast cells was similar to the pathogenesis of FTL mutation-induced neurodegenerative diseases (e.g., neuroferritinopathy or hereditary ferritinopathy), in which dysfunctional FTL increases iron accumulation in the cytoplasm and iron-mediated oxidative stress, thereby leading to iron-dependent cell death (ferroptosis) [22,41].

Animal experiments showed that knockdown of FTL-induced ferroptosis affected uterine spiral artery remodelling and was involved in the pathogenesis of PE. To further confirm our hypothesis, in vitro experiments were performed. Here, we found that FTL deficiency-induced trophoblast cell death was the dominant and central event, although FTL deficiency could also influence EMT and trophoblast cell invasion/migration to some extent (Fig. 5). Subsequently, this was greatly strengthened by the data from RNA sequencing in the FTL-downregulated trophoblast cells, i.e., the signalling molecules that regulate cell death were among the top two differentially expressed genes (Fig. 6).

Next, we tried to distinguish which kinds of cell death played a major role in FTL deficiency-induced trophoblast cell death by blocking various cell death with different types of inhibitors. The results showed that blocking ferroptosis with Fer-1 could obviously reverse shFTL-

induced cell death and improve trophoblast cell invasion/migration, while the comprehensive ferroptosis-related indices (e.g., ACSL4, GPX4, SLC7A11, FTH1, cell viability, MDA concentration, GSH concentration, $Fe^{2+}$ concentration, mitochondrial structure) [42] could be reversed by Fer-1 addition (Fig. 6 and Supplementary Fig. 7). These findings suggest that ferroptosis is a major form of trophoblast cell death in the context of FTL deficiency. However, it should be noted that we could not completely exclude the other type of programmed cell death since there is cross-regulation between other types of programmed cell death and ferroptosis [43]. Actually, this conclusion (i.e., ferroptosis in the main body) was not surprising since FTL is just one subunit of ferritin, which plays an important role in basic cellular processes such as DNA replication and repair, gene regulation, and the respiratory chain [44]. Ferroptosis is closely associated with imbalances in various parts of iron metabolism, including iron uptake, storage, utilization, and efflux [45], so dysfunctional ferritin dramatically attenuates cellular antioxidant capability, thereby leading to ferroptosis [42].

Eventually, we demonstrated evidence for ferroptosis occurring in patients with PE; MDA concentration and iron level increased, while GPX activity and GSH concentration decreased compared to the control. Additionally, high expression of ACSL4 and low expression of GPX4 in chorionic villi in patients with PE all imply that ferroptosis indeed occurs extensively in PE patients. Furthermore, the two linear correlation analyses (i.e., ferroptosis and mean arterial pressure and ferroptosis and FTL levels in patients' serum) confirmed that there was a linear relationship between PE patients' states of illness and ferroptosis, which is closely associated with the FTL level in patients' serum (Fig. 7). There is no doubt that these studies in human samples verified the conclusion of experimental results from the rat model of FTL deficiency-induced ferroptosis in the pathogenesis of PE. What kinds of factors cause the reduction in FTL levels in maternal-fetal tissues? Regarding this question, numerous studies about the role of ferritin and its gene regulation could be a very good reference, in which ferritin acts as the key molecule in response to the oxidative stress that typifies inflammatory diseases, including neurodegenerative diseases [46]. Likewise, PE is widely accepted as a generalized inflammatory process, thereby culminating in placental dysfunction [47]. Therefore, there is widespread speculation that the change in ferritin expression is forged from the consequences of interacting with these inflammatory responses [46].

In the rat model, FTL knockdown was noted in the placenta after systemic injection via the tail vein of Ad-shFTL. We observed that pregnant rats with FTL knockdown had elevated blood pressure and proteinuria accompanied by characteristic preeclamptic renal lesions, whereas nonpregnant rats exhibited no such signs, suggesting that blood pressure effects and renal damage in our model required FTL-mediated placenta-derived factors (Fig. 2, Supplementary Fig. 3). Nonetheless, adenovirus delivered intravenously may lead to a global knockdown that influenced FTL expression in various cell types and organs; therefore, the PE-like symptoms may not solely derive from FTL deficiency in trophoblasts. Thus, further studies are required to obtain placental trophoblast-specific knockout mice by a lentiviral vector or a newly reported lab-engineered nanoparticle that contains a placenta-homing peptide [48–51]. In addition, placenta-specific FTL-deficient mice can be constructed from transgenic mice harbouring a Cre gene regulated by a trophoblast-specific promoter [48,52,53]. These methods could be extremely helpful for obtaining a deeper understanding of FTL in trophoblasts.

In summary, we first showed that FTL is expressed in fetal-derived trophoblasts and that its expression is reduced in chorionic villi and decidua, as well as serum levels, from the first trimester to the third trimester of pregnancy. In early pregnant rats with FTL knockdown by intravenously injecting adenoviruses expressing shRNA targeting FTL, we found PE-like phenotypes, implying a causal relationship between FTL downregulation and PE. In the context of FTL deficiency, we found that cell death, especially ferroptosis, predominantly resulted in defective uterine spiral artery remodelling in both the rat model and patients with PE. It is suggested that FTL could be a potential biomarker and therapeutic target for PE in the future, although more relevant work is still required to completely uncover the PE pathophysiological mechanism.

## Contributors

X.Y., Y.D., L.S., M.S., P.Z., Z.H., J.W., A.H., M.L., and J.L. designed and performed experiments. G.W., X.Y. and R.L. analysed results, made the figures, and wrote the manuscript. All authors reviewed and critically edited the manuscript.

## Declaration of competing interest

The authors declare no competing interests.

## Data availability

Data will be made available on request.

## Acknowledgements

I would like to thank the obstetricians of the first affiliated hospital of Jinan University for their support and assistance in this study, and thank all the pregnant women who participated in this study. This study was supported by the Pilot Specialist Construction Project-Obstetrics and Gynecology (No. 711008), Science and Technology Planning Project of Guangdong Province of China (No. 2022A1515012139), NSFC grants (No. 32170825, 31971108 and 31771331), the Fundamental Research Funds for the Central Universities (No. 21621106), Guangdong Province Medical Science and Technology Research Fund Project (A2021056) and the Clinical Frontier Technology Program of the First Affiliated Hospital of Jinan University, China (No. JNU1AF-CFTP-2022-a01209).

## Appendix A. Supplementary data

Supplementary data to this article can be found online at https://doi.org/10.1016/j.redox.2022.102555.

## References

[1] L. Duley, Maternal mortality associated with hypertensive disorders of pregnancy in Africa, Asia, Latin America and the Caribbean, BJOG An Int. J. Obstet. Gynaecol. 99 (7) (1992) 547–553.
[2] N. Docheva, G. Arenas, K.M. Nieman, J. Lopes-Perdigao, K.J. Yeo, S. Rana, Angiogenic biomarkers for risk stratification in women with preeclampsia, Clin. Chem. 68 (6) (2022) 771–781.
[3] N. Al-Jameil, F.A. Khan, M.F. Khan, H. Tabassum, A brief overview of preeclampsia, J. Clin. Med. Res. 6 (1) (2014) 1.
[4] H. Valensise, B. Vasapollo, G. Gagliardi, G.P. Novelli, Early and late preeclampsia: two different maternal hemodynamic states in the latent phase of the disease, Hypertension 52 (5) (2008) 873–880.
[5] Long-term complications of preeclampsia, in: D. Williams (Ed.), Seminars in Nephrology, Elsevier, 2011.
[6] S. Bhattacharya, D.M. Campbell, The incidence of severe complications of preeclampsia, Hypertens. Pregnancy 24 (2) (2005) 181–190.
[7] C.W. Redman, G.P. Sacks, I.L. Sargent, Preeclampsia: an excessive maternal inflammatory response to pregnancy, Am. J. Obstet. Gynecol. 180 (2) (1999) 499–506.
[8] B. Formby, Immunologic response in pregnancy: its role in endocrine disorders of pregnancy and influence on the course of maternal autoimmune diseases, Endocrinol Metab. Clin. N. Am. 24 (1) (1995) 187–205.
[9] L.C. Chappell, C.A. Cluver, J. Kingdom, S. Tong, Pre-eclampsia, Lancet 398 (10297) (2021) 341–354.
[10] J.H. Veerbeek, L. Brouwers, M.P. Koster, S.V. Koenen, E.O. van Vliet, P.G. Nikkels, et al., Spiral artery remodeling and maternal cardiovascular risk: the spiral artery remodeling (SPAR) study, J. Hypertens. 34 (8) (2016) 1570–1577.
[11] H. Li, H. Ohta, Y. Tahara, S. Nakamura, K. Taguchi, M. Nakagawa, et al., Artificial oxygen carriers rescue placental hypoxia and improve fetal development in the rat pre-eclampsia model, Sci. Rep. 5 (1) (2015) 1–9.
[12] A. Robson, L.K. Harris, B.A. Innes, G.E. Lash, M.M. Aljunaidy, J.D. Aplin, et al., Uterine natural killer cells initiate spiral artery remodeling in human pregnancy, Faseb. J. 26 (12) (2012) 4876–4885.

[13] M. Kanat-Pektas, U. Yesildager, N. Tuncer, D.T. Arioz, G. Nadirgil-Koken, M. Yilmazer, Could mean platelet volume in late first trimester of pregnancy predict intrauterine growth restriction and pre-eclampsia? J. Obstet. Gynaecol. Res. 40 (7) (2014) 1840–1845.
[14] C. Arthuis, A. Novell, J.-M. Escoffre, F. Patat, A. Bouakaz, F. Perrotin, New insights into uteroplacental perfusion: quantitative analysis using Doppler and contrast-enhanced ultrasound imaging, Placenta 34 (5) (2013) 424–431.
[15] S.J. Dixon, K.M. Lemberg, M.R. Lamprecht, R. Skouta, E.M. Zaitsev, C.E. Gleason, et al., Ferroptosis: an iron-dependent form of nonapoptotic cell death, Cell 149 (5) (2012) 1060–1072.
[16] K. Bersuker, J.M. Hendricks, Z. Li, L. Magtanong, B. Ford, P.H. Tang, et al., The CoQ oxidoreductase FSP1 acts parallel to GPX4 to inhibit ferroptosis, Nature 575 (7784) (2019) 688–692.
[17] T.S. Anthonymuthu, Y.Y. Tyurina, W.-Y. Sun, K. Mikulska-Ruminska, I. H. Shrivastava, V.A. Tyurin, et al., Resolving the paradox of ferroptotic cell death: ferrostatin-1 binds to 15LOX/PEBP1 complex, suppresses generation of peroxidized ETE-PE, and protects against ferroptosis, Redox Biol. 38 (2021), 101744.
[18] H-f Yan, T. Zou, Q-z Tuo, S. Xu, H. Li, A.A. Belaidi, et al., Ferroptosis: mechanisms and links with diseases, Signal Transduct. Targeted Ther. 6 (1) (2021) 1–16.
[19] N. Zhang, X. Yu, J. Xie, H. Xu, New insights into the role of ferritin in iron homeostasis and neurodegenerative diseases, Mol. Neurobiol. 58 (6) (2021) 2812–2823.
[20] A.R. Curtis, C. Fey, C.M. Morris, L.A. Bindoff, P.G. Ince, P.F. Chinnery, et al., Mutation in the gene encoding ferritin light polypeptide causes dominant adult-onset basal ganglia disease, Nat. Genet. 28 (4) (2001) 350–354.
[21] K. Nishida, H.J. Garringer, N. Futamura, I. Funakawa, K. Jinnai, R. Vidal, et al., A novel ferritin light chain mutation in neuroferritinopathy with an atypical presentation, J. Neurol. Sci. 342 (1–2) (2014) 173–177.
[22] R. Vidal, L. Miravalle, X. Gao, A.G. Barbeito, M.A. Baraibar, S.K. Hekmatyar, et al., Expression of a mutant form of the ferritin light chain gene induces neurodegeneration and iron overload in transgenic mice, J. Neurosci. 28 (1) (2008) 60–67.
[23] M.A. Brown, L.A. Magee, L.C. Kenny, S.A. Karumanchi, F.P. McCarthy, S. Saito, et al., Hypertensive disorders of pregnancy: ISSHP classification, diagnosis, and management recommendations for international practice, Hypertension 72 (1) (2018) 24–43.
[24] A. He, J. Wang, X. Yang, J. Liu, X. Yang, G. Wang, et al., Screening of differentially expressed proteins in placentas from patients with late-onset preeclampsia, Proteonomics Clin. Appl. 16 (2) (2022), 2100053.
[25] B. Bewig, W.E. Schmidt, Accelerated titering of adenoviruses, Biotechniques 28 (5) (2000) 870–873.
[26] X. Fang, Z. Cai, H. Wang, D. Han, Q. Cheng, P. Zhang, et al., Loss of cardiac ferritin H facilitates cardiomyopathy via Slc7a11-mediated ferroptosis, Circ. Res. 127 (4) (2020) 486–501.
[27] G. Douglas, J.K. Bendall, M.J. Crabtree, A.L. Tatham, E.E. Carter, A.B. Hale, et al., Endothelial-specific Nox2 overexpression increases vascular superoxide and macrophage recruitment in ApoE−/− mice, Cardiovasc. Res. 94 (1) (2012) 20–29.
[28] L.A. Freitas, G.L. Mota, H.V.R. Silva, L.D.M. Silva, Two-dimensional sonographic and Doppler changes in the uteri of bitches according to breed, estrus cycle phase, parity, and fertility, Theriogenology 95 (2017) 171–177.
[29] K. Bibeau, B. Sicotte, M. Béland, M. Bhat, L. Gaboury, R. Couture, et al., Placental underperfusion in a rat model of intrauterine growth restriction induced by a reduced plasma volume expansion, PLoS One 11 (1) (2016), e0145982.
[30] I. Caniggia, H. Mostachfi, J. Winter, M. Gassmann, S.J. Lye, M. Kuliszewski, et al., Hypoxia-inducible factor-1 mediates the biological effects of oxygen on human trophoblast differentiation through TGFβ 3, J. Clin. Invest. 105 (5) (2000) 577–587.
[31] J. Liu, L. Gao, N. Zhan, P. Xu, Ja Yang, Fe Yuan, et al., Hypoxia induced ferritin light chain (FTL) promoted epithelia mesenchymal transition and chemoresistance of glioma, J. Exp. Clin. Cancer Res. 39 (1) (2020) 1–17.
[32] X. Liu, F. Qian, Q. Fan, L. Lin, M. He, P. Li, et al., NF-κB activation impedes the transdifferentiation of hypertrophic chondrocytes at the growth plate of mouse embryos in diabetic pregnancy, J. orthop. translat. 31 (2021) 52–61.
[33] F.B. Fromowitz, M.V. Viola, S. Chao, S. Oravez, Y. Mishriki, G. Finkel, et al., Ras p21 expression in the progression of breast cancer, Hum. Pathol. 18 (12) (1987) 1268–1275.
[34] F. Dong, P. Xiao, X. Li, P. Chang, W. Zhang, L. Wang, Cadmium triggers oxidative stress and mitochondrial injury mediated apoptosis in human extravillous trophoblast HTR-8/SVneo cells, Reprod. Toxicol. 101 (2021) 18–27.
[35] J. Pijuan, C. Barceló, D.F. Moreno, O. Maiques, P. Sisó, R.M. Marti, et al., In vitro cell migration, invasion, and adhesion assays: from cell imaging to data analysis, Front. Cell Dev. Biol. 107 (2019).
[36] H.S. Ko, S.K. Choi, H.K. Kang, H.S. Kim, J.H. Jeon, I.Y. Park, et al., Oncostatin M stimulates cell migration and proliferation by down-regulating E-cadherin in HTR8/SVneo cell line through STAT3 activation, Reprod. Biol. Endocrinol. 11 (1) (2013) 1–11.
[37] Z.-N. Huang, H.M. Chung, S.-C. Fang, L.-S. Her, Adhesion regulating molecule 1 mediates hap40 overexpression-induced mitochondrial defects, Int. J. Biol. Sci. 13 (11) (2017) 1420.
[38] S.A. Karumanchi, I.E. Stillman, In Vivo Rat Model of Preeclampsia, Placenta and Trophoblast: Springer, 2006, pp. 393–399.
[39] F. Spaans, B. Melgert, C. Chiang, T. Borghuis, P.A. Klok, P. de Vos, et al., Extracellular ATP decreases trophoblast invasion, spiral artery remodeling and immune cells in the mesometrial triangle in pregnant rats, Placenta 35 (8) (2014) 587–595.
[40] T. Cotechini, M. Komisarenko, A. Sperou, S. Macdonald-Goodfellow, M.A. Adams, C.H. Graham, Inflammation in rat pregnancy inhibits spiral artery remodeling leading to fetal growth restriction and features of preeclampsia, J. Exp. Med. 211 (1) (2014) 165–179.
[41] S. Li, Y. Huang, Ferroptosis: an iron-dependent cell death form linking metabolism, diseases, immune cell and targeted therapy, Clin. Transl. Oncol. (2021) 1–12.
[42] A. Ashraf, J. Jeandriens, H.G. Parkes, P.-W. So, Iron dyshomeostasis, lipid peroxidation and perturbed expression of cystine/glutamate antiporter in Alzheimer's disease: evidence of ferroptosis, Redox Biol. 32 (2020), 101494.
[43] Y. Xie, W. Hou, X. Song, Y. Yu, J. Huang, X. Sun, et al., Ferroptosis: process and function, Cell Death Differ. 23 (3) (2016) 369–379.
[44] M.C. Sammarco, S. Ditch, A. Banerjee, E. Grabczyk, Ferritin L and H subunits are differentially regulated on a post-transcriptional level, J. Biol. Chem. 283 (8) (2008) 4578–4587.
[45] X. Chen, C. Yu, R. Kang, D. Tang, Iron metabolism in ferroptosis, Front. Cell Dev. Biol. 8 (2020), 590226.
[46] F.M. Torti, S.V. Torti, Regulation of ferritin genes and protein, Blood 99 (10) (2002) 3505–3516.
[47] M.B. Tenório, R.C. Ferreira, F.A. Moura, N.B. Bueno, A.C.M. de Oliveira, M.O. F. Goulart, Cross-talk between oxidative stress and inflammation in preeclampsia, Oxid. Med. Cell. Longev. 2019 (2019), 8238727.
[48] T. Tobita, D. Kiyozumi, M. Ikawa, Placenta-specific gene manipulation using lentiviral vector and its application, Placenta 59 (Suppl 1) (2017) S37–s43.
[49] B. Zhang, L. Tan, Y. Yu, B. Wang, Z. Chen, J. Han, et al., Placenta-specific drug delivery by trophoblast-targeted nanoparticles in mice, Theranostics 8 (10) (2018) 2765–2781.
[50] N. Cureton, I. Korotkova, B. Baker, S. Greenwood, M. Wareing, V.R. Kotamraju, et al., Selective targeting of a novel vasodilator to the uterine vasculature to treat impaired uteroplacental perfusion in pregnancy, Theranostics 7 (15) (2017) 3715–3731.
[51] F. Beards, L.E. Jones, J. Charnock, K. Forbes, L.K. Harris, Placental homing peptide-microRNA inhibitor conjugates for targeted enhancement of intrinsic placental growth signaling, Theranostics 7 (11) (2017) 2940–2955.
[52] S. Kong, G. Liang, Z. Tu, D. Chen, H. Wang, J. Lu, Generation of Elf5-Cre knockin mouse strain for trophoblast-specific gene manipulation, Genesis 56 (4) (2018), e23101.
[53] C.C. Zhou, J. Chang, T. Mi, S. Abbasi, D. Gu, L. Huang, et al., Targeted expression of Cre recombinase provokes placental-specific DNA recombination in transgenic mice, PLoS One 7 (2) (2012), e29236.